Active Manipulation of Elastic Rods using Optimization-based Shape Perception and Sensorimotor Model Approximation

Guangfu Ma [1], Jiaming Qi [1], Yueyong Lv [1], Haibin, Zeng [1]
1. Harbin Institute of Technology, Harbin 150001, P. R. China
E-mail: qijm.hit@gmail.com

Abstract: Deformable object manipulation (DOM) remains challenging in robotics since the physical characteristics of deformable linear objects (DLO) are generally strongly nonlinear and unknown. This paper presents an active deformation framework for robot manipulating the elastic rod. The optimization-based curve fitting method is designed to extract a low-dimensional feature vector representing the three-dimensional centerline of the elastic rod. Deformation Jacobian Matrix (DJM) connecting feature changes and robot motion changes is estimated online by Adaptive Kalman Filter (AKF). The model-free velocity controller is designed based on the optimization criterion to accelerate the deformation speed of the elastic rod. The stability of the proposed manipulation framework and the boundedness of all signals in the closed-loop system are proved by Lyapunov theory. Detailed simulations are given to evaluate the performance of the proposed approach.

Key Words: Robotics, Shape-servoing, Deformable Objects, Sensor-based Control, Adaptive Kalman Filter

1 Introduction

Deformable object manipulation (DOM) has excellent application values in the field of robotics, such as assembling devices [1], manipulating cables [2], and folding clothes [3]. Improving the flexibility and accuracy of manipulating deformable linear objects (DLO) can help increase the automation of robots in real-world environments. Although there has been a lot of research in DOM, the following problems still exist: (i) Effective perception of shapes in a compact manner; (ii) Approximation of the shape-motion sensorimotor model; (iii) Design of deformation controller enabling the robot to conduct DOM. This work aims to present a unified solution to the above issues.

It is necessary to design a low-dimensional feature for adequate shape perception within an efficient manner in *shape servoing* (i.e., the automatic manipulation of DLO using robot) [4, 5]. Four simple features (point, distance, angle, and curvature) were used in [6] to quantify DLO; however, they can only represent local information without considering the whole shape. A constant curvature model was utilized to conduct the shape recognition of soft objects [7]. Truncated Fourier series was used in [8] to generate variable-dimensional features to represent the shapes, which is the first application of curve fitting (i.e., weight summation of a series of fixed functions named after basis functions [9]) in DOM. With the research of intelligent optimization algorithms, such methods have been increasingly used in curve fitting. Particle Swarm Optimization (PSO) was used to optimize the parameters of B-spline curves [10]. Simulated Annealing Algorithm (SAA) was utilized to solve optimal node parameters of NURBS for curve fitting [11]. Ant Colony Optimization (ACO) was used to optimize the center of RBF neural work to fit the given function [12]. Genetic Algorithm (GA) was adopted to optimize the parameters of Bezier-based mathematical model constructed by least square method [13]. Although optimization-based techniques have significantly improved curve fitting, they have not yet been applied in DOM.

Deformation Jacobian Matrix (DJM) is defined as a velocity mapping indicator between feature changes and motion changes of the robot [14]. As the strong nonlinearity of DLO, it is difficult to solve the DJM by analytical methods. Instead, most work of numerical methods have been applied. For example, Broyden update rules was used to approximate the deformation behavior between a continuum manipulator and an anisotropic deformable phantom [15]. Least Square Method (LSM) was used to estimate DJM, however its accuracy depends on the regression matrix [16]. Weighted LSM with a sliding-window was utilized to estimate DJM, which is robust to observation noise [17]. Kalman filter (KF) can use the previous state and current measurement value to obtain the optimal current state estimation, which is a simple calculation structure. Linear KF was used to estimation the image Jacobian matrix in visual servoing with good identification performance [18]. Although the KF-based methods have good potential in estimating DJM, they are rarely used.

Since the model properties of DLO are usually unknown, many model-based control methods are difficult to apply without model approximation. Model-free methods are well known to implement simply without prior physical structure of DLO, e.g., negative-feedback controller [19], and rolling-time domain predictive controller [20]. Based on ensuring the simplicity of the controller structure, it is also necessary to accelerate the deformation speed of the DLO object, which is a key consideration. Model-free shaping controllers are a hot research direction in DOM.

In this paper, we present an active deformation framework of the rigid robot manipulating the elastic rod and simultaneously approximating the sensorimotor model. An optimization-based feature extraction technique is constructed with radial regression parameterization to represent the three-dimensional centerline. Adaptive Kalman Filter (AKF) is used to approximate the quasi-deformation properties between features of DLO and robot motion. Detailed simulations are presented to validate the proposed method.

This work is supported by National Key Research and Development Program of China, 2020YFB1506700, Funded by Science and Technology on Space Intelligent Control Laboratory, No. HTKJ2020KL502014, and National Natural Science Foundation (NNSF) of China under Grant 12150008, 61973100, 61876050.

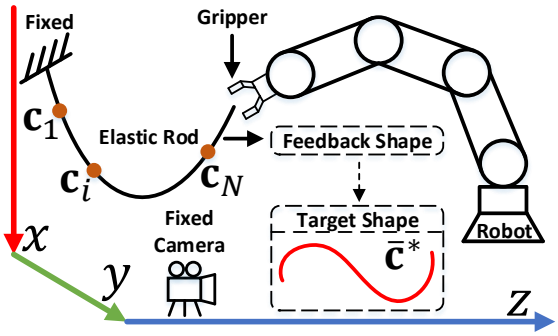

Fig. 1: Conceptual representation of the manipulation of the elastic rod. A fixed camera measures the three-dimensional centerline of the elastic rod. The task is defined as moving the robot to deform the elastic rod such its feedback $\bar{\mathbf{c}}$ approaches the desired shape configuration $\bar{\mathbf{c}}^*$ automatically.

2 Preliminaries

Notation. Bold small letters $\mathbf{m}$ and bold capital letters $\mathbf{M}$ represent column vectors and matrices. The subscript k denotes the discrete instant of the variable $\mathbf{x}_k$. $\mathbf{I}_n$ is an identity matrix with the dimension of $n \times n$. Kronecker product is defined by $\otimes$.

Some assumptions are given to derive our framework:

- A fixed depth camera in an eye-to-hand configuration measures the three-dimensional centerline of the rod (depicted in Fig. 1), which is defined by:

$$\bar{\mathbf{c}} = \left[\mathbf{c}_1^T, \ldots, \mathbf{c}_N^T\right]^T \in \mathbb{R}^{3N} \tag{1}$$

  where N is the number of points comprising the centerline, $\mathbf{c}_i = [c_{xi}, c_{yi}, c_{zi}]^T \in \mathbb{R}^3$ is the Cartesian coordinates of the ith $(i = 1, \cdots, N)$ center-point.
- The robot has kinematic control interface [21], and can accurately execute the given velocity command $\Delta\mathbf{r}_k \in \mathbb{R}^q$ that satisfies the incremental position signal $\mathbf{r}_k = \mathbf{r}_{k-1} + \Delta\mathbf{r}_k$.
- The rod is deformed gently such that the potential/elastic energy exclusively determines its shape.

Problem Statement. Given a three-dimensional target centerline $\bar{\mathbf{c}}^*$, design a vision-based velocity command $\Delta\mathbf{r}_k$ to enable the robot to deform the elastic rod into the target configuration, without the physical properties of the elastic rod and the calibration of the camera.

3 Methods

3.1 Feedback Shape Parameters

As the large dimension $3N$ of the raw coordinates $\bar{\mathbf{c}}$, it is not suitable for real-time control. Therefore, it is necessary to design a feature extraction technique to represent the shape of the elastic rod with a reduced-dimensional feature vector $\mathbf{s} \in \mathbb{R}^p$. In this section, we fit the centerline $\bar{\mathbf{c}}$ to a continuous parametric curve $\mathbf{f}(\rho) \in \mathbf{R}^3$ where ρ is the normalized arc-length between the start point $\mathbf{c}_1$ and the point $\mathbf{c}_i$ along the rod. Then, $\mathbf{c}_i = \mathbf{f}(\rho_i)$ where $0 \leq \rho_i \leq 1, \rho_1 = 0, \rho_N = 1$. The parametric curve is given as follows:

$$\mathbf{f}(\rho) = \sum_{j=0}^{n} \mathbf{p}_j G_j(\rho), \quad G_j(\rho) = \exp(-j|\rho|^2) \tag{2}$$

where $n \in \mathbb{N}^*$ is the fitting order, and $\mathbf{p}_j \in \mathbb{R}^3$ represents shape parameters. $G_j(\rho)$ is the radial basis regression parameterization with $j \in [0, n]$ determining its width. To determine the parameters $\mathbf{p}_j$, a fitness function based on Akaikes Information Criterion (AIC) (originally used to evaluate the accuracy of the model for a set of data) by referring to (2) is proposed as follows:

$$\mathrm{AIC} = \ln((\mathbf{G}\mathbf{s} - \bar{\mathbf{c}})^T (\mathbf{G}\mathbf{s} - \bar{\mathbf{c}}) + 1) + 3n \tag{3}$$

where $\mathbf{G}$ and $\mathbf{s}$ are defined as follows:

$$\begin{aligned} \mathbf{G} &= [\mathbf{G}_1^T, \ldots, \mathbf{G}_N^T]^T \in \mathbb{R}^{3N \times 3(n+1)} \\ \mathbf{G}_i &= [G_0(\rho_i), \ldots, G_n(\rho_i)] \otimes \mathbf{I}_3 \in \mathbb{R}^{3 \times 3(n+1)} \\ \mathbf{s} &= [\mathbf{p}_0^T, \ldots, \mathbf{p}_n^T]^T \in \mathbb{R}^{3(n+1)} \end{aligned} \tag{4}$$

The first term in (3) is utilized to evaluate the fitting performance between the approximated shape $\mathbf{G}\mathbf{s}$ and the feedback shape $\bar{\mathbf{c}}$, the constant bias 1 is used to prevent singularity in logarithmic computation. The last term penalizes the increase in n. Our goal is to minimize (3) to identify $\mathbf{s}$ to represent the centerline $\bar{\mathbf{c}}$ adequately. For this issue, analytical methods can be used, e.g., the least-squares method. However, the traditional analytical method will affect the error of the fitting. It is difficult to obtain an analytical solution, especially when the fitting function is complicated (e.g., trigonometric, logarithmic, and exponential). In this paper, the optimization-based algorithms are adopted to solve the shape parameters $\mathbf{p}_j$ of (3) without complex calculations and a prior analytical structure. Generally used optimization algorithms are as follows:

- GA has global searchability without falling into the trap of rapid descent of locally optimal solutions [22];
- PSO is simpler than GA and can find the global optimum with a strong global search ability for nonlinear and multivariable problems [23];
- SAA is capable of avoiding the optimal local solution and finding the global minimum solution in the sense of probability by random search technology [24];
- ACO adopts a heuristic probability search method and a distributed parallel computing manner, improving computational efficiency and avoiding falling into the local optimum [25].

Applying the above optimization algorithms on (3), we can get the optimal $\mathbf{s}$ which can be used to represent the three-dimensional feedback centerline $\bar{\mathbf{c}}$ of the elastic rod.

3.2 Approximation of Deformation Jacobian Matrix

In this paper, the quasi-static manipulation of the elastic rod is considered. The robot pose $\mathbf{r}$ directly affects the centerline $\bar{\mathbf{c}}$ of the elastic rod, which can be described by the unknown nonlinear function, i.e., $\bar{\mathbf{c}} = \mathbf{f}_c(\mathbf{r})$. According to (3), there is an unknown optimal mapping between $\mathbf{s}$ and $\bar{\mathbf{c}}$, i.e., $\mathbf{s} = \mathbf{f}_s(\bar{\mathbf{c}})$. Thus, the cascaded kinematic model from $\mathbf{r}$ to $\mathbf{s}$ can be obtained by: $\mathbf{s} = \mathbf{f}_s(\mathbf{f}_c(\mathbf{r}))$. Differentiating this model concerning time t, it yields

$$\dot{\mathbf{s}} = \mathbf{J}(t)\dot{\mathbf{r}} \tag{5}$$

where $\mathbf{J}(t) = \partial\mathbf{s}/\partial\mathbf{r} \in \mathbb{R}^{p \times q}$ is the deformation Jacobian matrix (DJM), which describes the velocity mapping associating $\mathbf{s}$ and $\mathbf{r}$. As the deformation properties of the elastic rod

are unknown, thus DJM cannot be analytically computed. Discretizing (5) yields the first-order difference equation:

$$\mathbf{s}_k = \mathbf{s}_{k-1} + \mathbf{J}_k \cdot \Delta\mathbf{r}_k \tag{6}$$

Define the state $\mathbf{x}_k = [\partial s_1/\partial \mathbf{r}, \ldots, \partial s_p/\partial \mathbf{r}]^T \in \mathbb{R}^{pq}$ where $\partial s_i/\partial \mathbf{r} \in \mathbb{R}^{1\times q}$ is the ith row of $\mathbf{J}_k$. Afterwards, the discrete system (6) can be transformed into the linear stochastic system with no control input:

$$\mathbf{x}_k = \mathbf{x}_{k-1} + \mathbf{w}_k, \;\; \mathbf{y}_k = \mathbf{M}_k \cdot \mathbf{x}_k + \mathbf{v}_k \tag{7}$$

where $\mathbf{y}_k = \Delta\mathbf{s}_k = \mathbf{s}_k - \mathbf{s}_{k-1}$ is the system output. $\mathbf{M}_k$ is the measurement matrix defined by:

$$\mathbf{M}_k = \mathrm{diag}\left(\Delta\mathbf{r}_k^T, \cdots, \Delta\mathbf{r}_k^T\right) \in \mathbb{R}^{p\times pq} \tag{8}$$

where $\mathbf{w}_k$ and $\mathbf{v}_k$ are the process noise and measurement noise, respectively, which have the statistical properties:

$$\begin{aligned} E[\mathbf{w}_k] = \pi_k,\; E[\mathbf{v}_k] = \varpi_k,\; E[\mathbf{w}_k\mathbf{v}_j^T] = 0, \\ E[\mathbf{w}_k\mathbf{w}_j^T] = \Phi_k\delta_{kj},\; E[\mathbf{v}_k\mathbf{v}_j^T] = \Psi_k\delta_{kj} \end{aligned} \tag{9}$$

where Φ_k and Ψ_k are the covariance matrices for $\mathbf{w}_k$ and $\mathbf{v}_k$, respectively, and δ_{kj} is a Kronecker-δ function [26]. Traditional KF [18] requires that $\mathbf{w}_k$ and $\mathbf{v}_k$ are known Gaussian white noise. However, during the estimation process, the statistical properties of $\mathbf{w}_k$ and $\mathbf{v}_k$ may change. Thus, it cannot be considered that $\mathbf{w}_k$ and $\mathbf{v}_k$ is Gaussian white noise. For this issue, AKF [26] is utilized to compute the local estimation of $\mathbf{J}_k$ with approximating noise parameters simultaneously. The procedure can be summarized as follows:

Step 1: Prediction.

$$\hat{\mathbf{x}}_{k,k-1} = \hat{\mathbf{x}}_{k-1} + \hat{\pi}_{k-1},\; \mathbf{P}_{k,k-1} = \mathbf{P}_{k-1} + \hat{\Phi}_{k-1} \tag{10}$$

Step 2: Correction.

$$\begin{aligned} \mathbf{K}_k &= \mathbf{P}_{k,k-1}\mathbf{M}_k^T\left(\mathbf{M}_k\mathbf{P}_{k,k-1}\mathbf{M}_k^T + \hat{\Psi}_{k-1}\right)^{-1} \\ \tilde{\mathbf{y}}_k &= \mathbf{y}_k - \mathbf{M}_k\hat{\mathbf{x}}_{k,k-1} - \hat{\varpi}_{k-1} \\ \hat{\mathbf{x}}_k &= \hat{\mathbf{x}}_{k,k-1} + \mathbf{K}_k\tilde{\mathbf{y}}_k \\ \mathbf{P}_k &= \left(\mathbf{I}_{3p} - \mathbf{K}_k\mathbf{M}_k\right)\mathbf{P}_{k,k-1} \end{aligned} \tag{11}$$

Step 3: Update

$$\begin{aligned} \hat{\pi}_k &= (1-\varepsilon)\,\hat{\pi}_{k-1} + \varepsilon\left(\hat{\mathbf{x}}_k - \hat{\mathbf{x}}_{k-1}\right) \\ \hat{\varpi}_k &= (1-\varepsilon)\,\hat{\varpi}_{k-1} + \varepsilon\left(\mathbf{y}_k - \mathbf{M}_k\hat{\mathbf{x}}_{k,k-1}\right) \\ \hat{\Phi}_k &= (1-\varepsilon)\,\hat{\Phi}_{k-1} + \varepsilon\left(\mathbf{K}_k\tilde{\mathbf{y}}_k\tilde{\mathbf{y}}_k^T\mathbf{K}_k^T + \mathbf{P}_k - \mathbf{P}_{k-1}\right) \\ \hat{\Psi}_k &= (1-\varepsilon)\,\hat{\Psi}_{k-1} + \varepsilon\left(\tilde{\mathbf{y}}_k\tilde{\mathbf{y}}_k^T - \mathbf{M}_k\mathbf{P}_k\mathbf{M}_k^T\right) \end{aligned} \tag{12}$$

where $0 < \varepsilon < 1$ is the forgetting factor.

Step 4: Repeat steps 1-3 for the next update.

Finally, once we get $\hat{\mathbf{x}}_k$ at each step, $\hat{\mathbf{J}}_k$ is updated online.

3.3 Shape Motion Controller

Assuming AKF has accurately estimated DJM at the time instant k, i.e., $\hat{\mathbf{J}}_k \approx \mathbf{J}_k$, such that the shape-motion difference model satisfies: $\mathbf{s}_k = \mathbf{s}_{k-1} + \hat{\mathbf{J}}_k \cdot \Delta\mathbf{r}_k$. In this section, the velocity command $\Delta\mathbf{r}_k$ is designed to guide the robot to deform the elastic rod such that its feedback shape $\bar{\mathbf{c}}$ approaches the constant desired shape $\bar{\mathbf{c}}^*$. The deformation error is defined by $\mathbf{e}_k = \mathbf{s}_k - \mathbf{s}^*$ between the feedback feature $\mathbf{s}_k$ and the target feature $\mathbf{s}^*$ representing $\bar{\mathbf{c}}^*$, and it yields

$$\mathbf{e}_k - \mathbf{e}_{k-1} = \hat{\mathbf{J}}_k\Delta\mathbf{r}_k, \mathbf{e}_k + \mathbf{e}_{k-1} = 2\mathbf{e}_{k-1} + \hat{\mathbf{J}}_k\Delta\mathbf{r}_k \tag{13}$$

For this issue, the quadratic performance index is presented as follows:

$$Q = \mathbf{e}_k^T\mathbf{e}_k + \Delta\mathbf{s}_k^T\Delta\mathbf{s}_k + \omega\Delta\mathbf{r}_k^T\Delta\mathbf{r}_k \tag{14}$$

where $\omega > 0$ is a weight factor, which regulates the amplitude and smoothness of $\Delta\mathbf{r}_k$. Note that if ω is too small, the system may oscillate or even lose stability. To this end, let us compute the partial derivative of (14) with respect to $\Delta\mathbf{r}_k$, and solve the expression for $\Delta\mathbf{r}_k$:

$$\Delta\mathbf{r}_k = -\mathbf{A}^{-1}\hat{\mathbf{J}}_k^T\mathbf{e}_{k-1}, \;\; \mathbf{A} = \omega\mathbf{I}_q + 2\hat{\mathbf{J}}_k^T\hat{\mathbf{J}}_k \tag{15}$$

Compared with the criterion index [27], the second term considers the influence of $\mathbf{s}_{k-1}$ on $\mathbf{s}_k$. When $\mathbf{s}_k$ deviates from $\mathbf{s}^*$, it takes into account the influence of $\Delta\mathbf{s}_k$ on the system, thereby accelerating the system to reach the target and overcoming the steady error. When the system is stable (i.e., $\Delta\mathbf{s}_k \approx 0$), this term is near to zero where it is similar to [27]. The flow diagram of the proposed manipulation framework is shown in Fig. 2.

Proposition 1. *Consider the closed-loop system consisting of the difference model (6), the model estimation algorithm (10)-(12), and the shape-motion controller (15). Given the desired shape $\mathbf{s}^*$, there exist appropriate design parameters such that all signals in the closed-loop system remain ultimately bounded, and the deformation error $\mathbf{e}_k$ converges to a compact set around zero.*

Proof. The discrete Lyapunov function is defined by $V_k = \frac{1}{2}\mathbf{e}_k^T\mathbf{e}_k$, whose discrete difference is [28]:

$$\Delta V_k = V_k - V_{k-1} = \frac{1}{2}\mathbf{e}_k^T\mathbf{e}_k - \frac{1}{2}\mathbf{e}_{k-1}^T\mathbf{e}_{k-1} \tag{16}$$

By substituting (13) into (16), it yields

$$\begin{aligned} \Delta V_k &= (\mathbf{e}_{k-1} + \tfrac{1}{2}\hat{\mathbf{J}}_k\Delta\mathbf{r}_k)^T\hat{\mathbf{J}}_k\Delta\mathbf{r}_k = -\mathbf{e}_{k-1}^T\mathbf{L}\mathbf{e}_{k-1} \\ \mathbf{L} &= \hat{\mathbf{J}}_k\mathbf{A}^{-1}(\omega\mathbf{I}_q + \tfrac{3}{2}\hat{\mathbf{J}}_k^T\hat{\mathbf{J}}_k)\mathbf{A}^{-1}\hat{\mathbf{J}}_k^T \end{aligned} \tag{17}$$

Throughout this paper, $\hat{\mathbf{J}}_k$ is assumed to be full column rank; therefore, the stability of the system is stable since $V_k > 0$ and $\Delta V_k \leq 0$. As $\mathbf{L}$ is never full rank; thus $\mathbf{L}$ is only symmetric semi-positive definite, which implies that $\|\mathbf{e}_k\|$ can only converge to a local region near zero. As AKF [26] is bounded in approximating DJM, with considering the boundedness of $\mathbf{e}_k$, thus $\Delta\mathbf{r}_k$ is bounded. By the above analyses, all signals in the closed-loop system remain bounded. For such shape manipulation tasks, the global asymptotic stability of $\mathbf{e}_k$ cannot be guaranteed [29]. □

4 Simulation Results

In this section, simulations are conducted to validate the effectiveness of the proposed framework. The three degree-of-freedom robot $\Delta\mathbf{r}_k = (\Delta r_1, \Delta r_2, \Delta r_3) \in \mathbb{R}^3$ rigidly

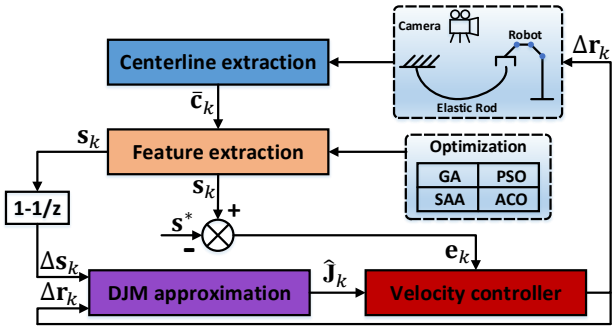

Fig. 2: The control workflow of the proposed manipulation framework.

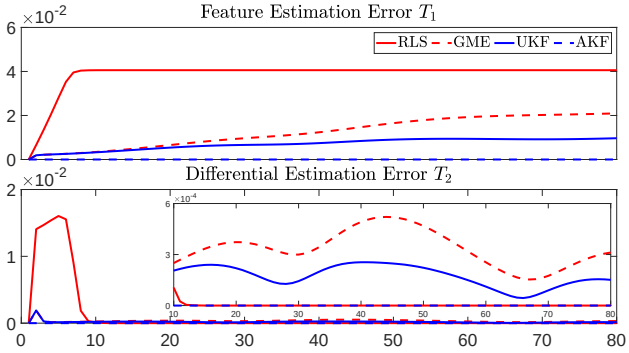

Fig. 4: Time evaluation of T_1 and T_2. The robot deforms the elastic rod along a given trajectory. The abscissa is the step.

grasps one end of an elastic rod, while maintaining other end fixed. The simulator of the elastic rod is designed referring to [30] by using the minimum energy principle [31]. This simulator is publicly available at https://github.com/q546163199/shape_deformation/. The number of center-points of the elastic rod is set to 20, i.e., $N = 20$. All numerical simulations are implemented in MATLAB.

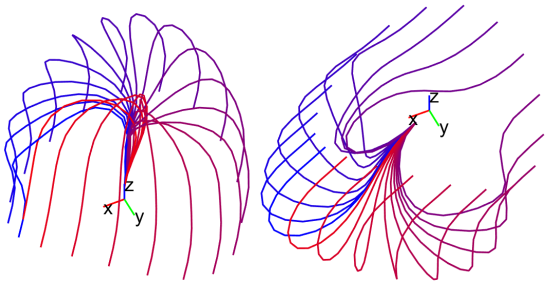

(a) Shape set-1 (b) Shape set-2

Fig. 3: Various shape sets generated by different robot configuration.

Table 1: Fitting comparison results among GA, PSO, SAA, ACO conducting with 100 shape sets

	n	G	s	Average time	Average error
GA	6	60×21	21	0.557s	0.007
PSO	6	60×21	21	0.263s	0.073
SAA	6	60×21	21	0.923s	0.278
ACO	6	60×21	21	0.436s	0.027

4.1 Feature Extraction Comparison

In this section, the robot deforms the elastic rod continuously to generate 100 shapes, which are used to validate the effectiveness of the proposed optimization-based feature extraction technique (3) among GA, PSO, SAA, and ACO.

Fig. 3 shows the sampled shapes among different robot motions. Table 1 shows the comparison results, including average computation time and the average error $(\bar{\mathbf{c}} - \mathbf{G}\mathbf{s})$ between the feedback shape $\bar{\mathbf{c}}$ and the reconstruction shape $\mathbf{G}\mathbf{s}$. PSO is the fastest, followed by ACO and GA, and SAA. Reducing the number of particles in the PSO can further enhance its computational efficiency. As for accuracy, GA has the best fitting performance, while SAA is the worst. Therefore, considering the trade balance between accuracy and speed, GA is used with $n = 6$ in the following sections.

4.2 Validation of the Sensorimotor Approximation

In this section, the elastic rod is manipulated by the robot along with a pre-defined trajectory (i.e., $\mathbf{r}_k$ and $\Delta\mathbf{r}_k$ are known) to evaluate the performance of AKF in approximating $\mathbf{J}_k$ combined with Recursive Least Square (RLS) [32] given in (18), Geman–McClure Estimator (GME) [20], and Unscented Kalman Filter (UKF) [33].

$$\begin{aligned}\hat{\mathbf{J}}_k &= \hat{\mathbf{J}}_{k-1} + \frac{(\Delta\mathbf{s}_k - \hat{\mathbf{J}}_{k-1}\Delta\mathbf{r}_k)\Delta\mathbf{r}_k^T\mathbf{U}_{k-1}}{\eta + \Delta\mathbf{r}_k^T\mathbf{U}_{k-1}\Delta\mathbf{r}_k} \\ \mathbf{U}_k &= \mathbf{U}_{k-1} - \frac{\mathbf{U}_{k-1}\Delta\mathbf{r}_k\Delta\mathbf{r}_k^T\mathbf{U}_{k-1}}{\eta + \Delta\mathbf{r}_k^T\mathbf{U}_{k-1}\Delta\mathbf{r}_k}\end{aligned} \tag{18}$$

where $0 < \eta \leq 1$ is a forgetting factor specifying the influence of past data on the estimation. The initialization of $\hat{\mathbf{J}}_0$ is: Given an arbitrary m-step linearly independent random motion at the initial position, $\Delta\mathbf{r}_1, \ldots, \Delta\mathbf{r}_m$, and observe the corresponding shape feature changes $\Delta\mathbf{s}_1, \ldots, \Delta\mathbf{s}_m$, finally it obtains: $\hat{\mathbf{J}}_0 = [\Delta\mathbf{s}_1, \ldots, \Delta\mathbf{s}_m][\Delta\mathbf{r}_1, \ldots, \Delta\mathbf{r}_m]^{-1}$. Two criteria are introduced to evaluate the approximation performance [34]:

$$T_1 = \|\hat{\mathbf{s}}_k - \mathbf{s}_k\|, \quad T_2 = \|\Delta\mathbf{s}_k - \hat{\mathbf{J}}_k\Delta\mathbf{r}_k\| \tag{19}$$

where $\hat{\mathbf{s}}_k$ is given by $\hat{\mathbf{s}}_k = \hat{\mathbf{s}}_{k-1} + \hat{\mathbf{J}}_k\Delta\mathbf{r}_k$, $\hat{\mathbf{s}}_0 = \mathbf{s}_0$.

Fig. 4 shows the evaluation curves of T_1 and T_2 during the estimation procedure. AKF has the smallest T_1, UKF and GME are the second-best, while RLS is the worst. This shows that the AKF can estimate the noise parameters and provide feedback to compensate for the estimation of DJM adequately. In terms of T_2, AKF still performs best without apparent fluctuations, which depicts that AKF can continuously estimate DJM accurately and embody the strong adaptive ability and robustness in different local regions. The above results prove that AKF can estimate DJM accurately and continuously.

4.3 Manipulation of Elastic Rods

In this section, the robot is commanded to deform the elastic rod into the target shape configuration. The accessibility of the desired shape is guaranteed by moving the robot to the specified position in advance and records. We show the deformation trajectories every three discrete steps to visually compare the manipulation performance.

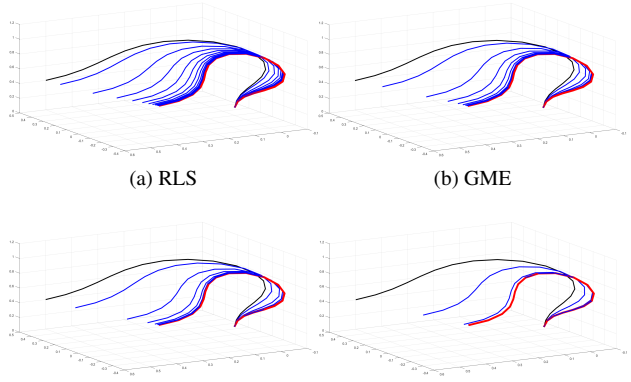

(a) RLS (b) GME (c) UKF (d) AKF

Fig. 5: The deformation trajectories of the elastic rod during the manipulation process within the controller (15) among RLS, GME, UKF, AKF. Solid black line, solid blue lines, and solid red line represent the initial, intermediate, and desired shapes, respectively.

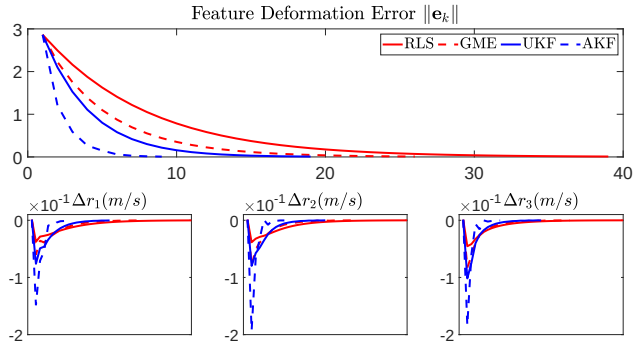

Fig. 6: Time evaluation of the deformation error $\|\mathbf{e}_k\|$ and the velocity command $\Delta\mathbf{r}_k$ during the manipulation process among RLS, GME, UKF, AKF. The abscissa is the step.

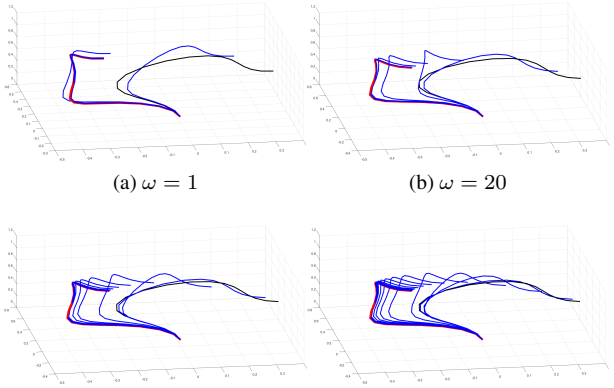

(a) $\omega = 1$ (b) $\omega = 20$ (c) $\omega = 50$ (d) $\omega = 100$

Fig. 7: The deformation trajectories of the elastic rod during the manipulation process within the controller (15) with different control parameter ω, i.e., $\omega = 1, \omega = 20, \omega = 50, \omega = 100$. Solid black line, solid blue lines, and solid red line represent the initial, intermediate, and desired shapes, respectively.

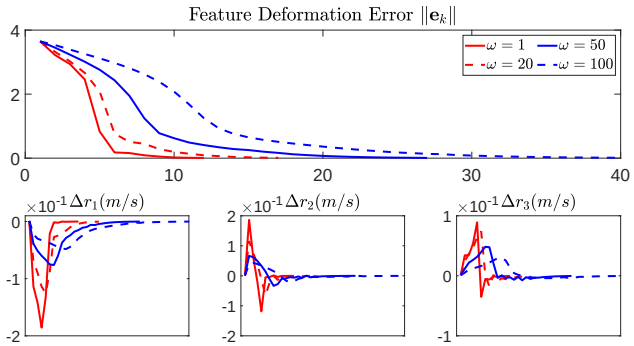

Fig. 8: Time evaluation of the deformation error $\|\mathbf{e}_k\|$ and the velocity command $\Delta\mathbf{r}_k$ during the manipulation process with different ω. The abscissa is the step.

First, the motion controller (15) is combined with RLS, GME, UKF, and AKF, respectively. Fig. 5 depicts the deformation trajectories of the elastic rod. The solid black line, solid blue lines, and solid red line represent the initial, transitional, and target shapes, respectively. As can be seen from Fig. 5, each DJM estimator can complete the manipulation within the controller (15). Fig. 6 depicts the deformation error $\|\mathbf{e}_k\|$ and the velocity command $\Delta\mathbf{r}_k$. AKF within (15) has the fastest convergence speed and can accurately estimate DJM and time-varying noise parameters, which generates an appropriate controller $\Delta\mathbf{r}_k$. And the proposed optimization-based feature extraction technique can well represent the centerline $\bar{\mathbf{c}}$ with a reduced-dimensional feature vector. This can be verified from Fig. 5, the feedback shape $\bar{\mathbf{c}}$ and the desired shape $\bar{\mathbf{c}}^*$ visually coincide.

Second, for the influence evaluation of control parameter ω on the controller (15), four cases ($\omega = 1, \omega = 20, \omega = 50, \omega = 100$) are given in Fig. 7 and Fig. 8. With the increase of ω, the convergence speed of $\mathbf{e}_k$ gradually decreases with a smoother control signal $\Delta\mathbf{r}_k$. Therefore, by adjusting ω, the system's dynamic characteristics can be regulated. In practice, there is a trade balance between the convergence speed of $\mathbf{e}_k$ and the smoothness of $\Delta\mathbf{r}_k$.

The above results show that the proposed manipulation framework (i.e., representation, approximation, and control) can perform the shape deformation task well with satisfying performance.

5 Conclusion

This paper presents a vision-based manipulation framework for the elastic rod without known physical properties. An optimization-based feature extraction technique is designed to represent the geometric centerline of the elastic rod with a low-dimensional feature. AKF is used to estimate DJM with time-varying noise matrices simultaneously iteratively; then, it is used to derive the shape-motion controller. The closed-loop system is proved to be stable with Lyapunov stability theory. The detailed simulations verify the effectiveness of the proposed framework. For future work, we will consider manipulating more complicated shapes and combining neural networks with our research to further compensate for shape perception.

References

[1] X. Li, X. Su, Y. Gao, and Y.-H. Liu, "Vision-based robotic grasping and manipulation of usb wires," in *2018 IEEE International Conference on Robotics and Automation (ICRA)*. IEEE, 2018, pp. 3482–3487.

[2] H. Wakamatsu, E. Arai, and S. Hirai, "Knotting/unknotting manipulation of deformable linear objects," *The International Journal of Robotics Research*, vol. 25, no. 4, pp. 371–395, 2006.

[3] S. Miller, J. Van Den Berg, M. Fritz, T. Darrell, K. Goldberg, and P. Abbeel, "A geometric approach to robotic laundry folding," *The International Journal of Robotics Research*, vol. 31, no. 2, pp. 249–267, 2012.

[4] J. Qi, G. Ma, J. Zhu, P. Zhou, Y. Lyu, H. Zhang, and D. Navarro-Alarcon, "Contour moments based manipulation of composite rigid-deformable objects with finite time model estimation and shape/position control," *IEEE/ASME Transactions on Mechatronics*, 2021.

[5] P. Zhou, J. Zhu, S. Huo, and D. Navarro-Alarcon, "Lasesom: A latent and semantic representation framework for soft object manipulation," *IEEE Robotics and Automation Letters*, vol. 6, no. 3, pp. 5381–5388, 2021.

[6] D. Navarro-Alarcon, H. M. Yip, Z. Wang, Y.-H. Liu, F. Zhong, T. Zhang, and P. Li, "Automatic 3-d manipulation of soft objects by robotic arms with an adaptive deformation model," *IEEE Transactions on Robotics*, vol. 32, no. 2, pp. 429–441, 2016.

[7] S. Zou, Y. Lv, Y. Man, and W. Han, "Design and implement of shape detection for the soft manipulator," in *2020 39th Chinese Control Conference (CCC)*. IEEE, 2020, pp. 3972–3977.

[8] D. Navarro-Alarcon and Y.-H. Liu, "Fourier-based shape servoing: A new feedback method to actively deform soft objects into desired 2-d image contours," *IEEE Transactions on Robotics*, vol. 34, no. 1, pp. 272–279, 2017.

[9] G. Trejo-Caballero, H. Rostro-Gonzalez, C. Garcia-Capulin, O. Ibarra-Manzano, J. Avina-Cervantes, and C. Torres-Huitzil, "Automatic curve fitting based on radial basis functions and a hierarchical genetic algorithm," *Mathematical Problems in Engineering*, vol. 2015, 2015.

[10] Z. Q.-s. Z. Ling-qiu and Q. H.-c. L. Ji, "Curve fitting of b-spline based on particle swarm optimization," *Computer Science*, 2009.

[11] M. Sarfraz and M. Riyazuddin, "Curve fitting with nurbs using simulated annealing," in *Applied Soft Computing Technologies: The Challenge of Complexity*. Springer, 2006, pp. 99–112.

[12] M. Chun-tao, L. Xiao-xia, and Z. Li-yong, "Radial basis function neural network based on ant colony optimization," in *2007 International Conference on Computational Intelligence and Security Workshops (CISW 2007)*. IEEE, 2007, pp. 59–62.

[13] L. Zhao, J. Jiang, C. Song, L. Bao, and J. Gao, "Parameter optimization for bezier curve fitting based on genetic algorithm," in *International conference in swarm intelligence*. Springer, 2013, pp. 451–458.

[14] D. Navarro-Alarcon, Y.-h. Liu, J. G. Romero, and P. Li, "On the visual deformation servoing of compliant objects: Uncalibrated control methods and experiments," *The International Journal of Robotics Research*, vol. 33, no. 11, pp. 1462–1480, 2014.

[15] F. Alambeigi, Z. Wang, R. Hegeman, Y.-H. Liu, and M. Armand, "Autonomous data-driven manipulation of unknown anisotropic deformable tissues using unmodelled continuum manipulators," *IEEE Robotics and Automation Letters*, vol. 4, no. 2, pp. 254–261, 2018.

[16] D. Navarro-Alarcon, Y.-H. Liu, J. G. Romero, and P. Li, "Model-free visually servoed deformation control of elastic objects by robot manipulators," *IEEE Transactions on Robotics*, vol. 29, no. 6, pp. 1457–1468, 2013.

[17] R. Lagneau, A. Krupa, and M. Marchal, "Active deformation through visual servoing of soft objects," in *2020 IEEE International Conference on Robotics and Automation (ICRA)*. IEEE, 2020, pp. 8978–8984.

[18] J. Qian and J. Su, "Online estimation of image jacobian matrix by kalman-bucy filter for uncalibrated stereo vision feedback," in *Proceedings 2002 IEEE International Conference on Robotics and Automation (Cat. No. 02CH37292)*, vol. 1. IEEE, 2002, pp. 562–567.

[19] D. Navarro-Alarcon, J. Qi, J. Zhu, and A. Cherubini, "A lyapunov-stable adaptive method to approximate sensorimotor models for sensor-based control," *Frontiers in Neurorobotics*, p. 59, 2020.

[20] H. Mo, B. Ouyang, L. Xing, D. Dong, Y. Liu, and D. Sun, "Automated 3-d deformation of a soft object using a continuum robot," *IEEE Transactions on Automation Science and Engineering*, vol. 18, no. 4, pp. 2076–2086, 2020.

[21] B. Siciliano, "Kinematic control of redundant robot manipulators: A tutorial," *Journal of intelligent and robotic systems*, vol. 3, no. 3, pp. 201–212, 1990.

[22] D. Whitley, "A genetic algorithm tutorial," *Statistics and computing*, vol. 4, no. 2, pp. 65–85, 1994.

[23] M. Clerc, *Particle swarm optimization*. John Wiley & Sons, 2010, vol. 93.

[24] E. Aarts, J. Korst, and W. Michiels, "Simulated annealing," in *Search methodologies*. Springer, 2005, pp. 187–210.

[25] T. Liao, T. Stützle, M. A. M. de Oca, and M. Dorigo, "A unified ant colony optimization algorithm for continuous optimization," *European Journal of Operational Research*, vol. 234, no. 3, pp. 597–609, 2014.

[26] R. Xiaolin, L. Hongwen, and L. Yuanchun, "Online image jacobian identification using optimal adaptive robust kalman filter for uncalibrated visual servoing," in *2017 2nd Asia-Pacific Conference on Intelligent Robot Systems (ACIRS)*. IEEE, 2017, pp. 53–57.

[27] D. Navarro-Alarcon, A. Cherubini, and X. Li, "On model adaptation for sensorimotor control of robots," in *2019 Chinese Control Conference (CCC)*. IEEE, 2019, pp. 2548–2552.

[28] S. Sarpturk, Y. Istefanopulos, and O. Kaynak, "On the stability of discrete-time sliding mode control systems," *IEEE Transactions on Automatic Control*, vol. 32, no. 10, pp. 930–932, 1987.

[29] J.-J. Slotine and W. Li, *Applied Nonlinear Control*, 1st ed. Upper Saddle River, NJ: Prentice Hall, 1991.

[30] H. Wakamatsu, "Modeling of linear objects considering bend, twist, and extensional deformation," *Proc.of IEEE Int.conf.robotics Automation*, 1995.

[31] D. Fleisch and L. Kinnaman, "A student's guide to lagrangians and hamiltonians," 2015.

[32] K. Hosoda and M. Asada, "Versatile visual servoing without knowledge of true jacobian," in *Proceedings of IEEE/RSJ International Conference on Intelligent Robots and Systems (IROS'94)*, vol. 1. IEEE, 1994, pp. 186–193.

[33] J. Qi, W. Ma, D. Navarro-Alarcon, H. Gao, and G. Ma, "Adaptive shape servoing of elastic rods using parameterized regression features and auto-tuning motion controls," *arXiv preprint arXiv:2008.06896*, 2020.

[34] J. Qi, G. Ma, P. Zhou, H. Zhang, Y. Lyu, and D. Navarro-Alarcon, "Towards latent space based manipulation of elastic rods using autoencoder models and robust centerline extractions," *Advanced Robotics*, pp. 1–15, 2021.